Double Trouble of Air Pollution by Anthropogenic Dust

Xia, Wenwen

2022-01-18

Xia , W , Wang , Y , Chen , S , Huang , J , Wang , B , Zhang , G J , Zhang , Y , Liu , X , Ma , J , Gong , P , Jiang , Y , Wu , M , Xue , J , Wei , L & Zhang , T 2022 , ' Double Trouble of Air Pollution by Anthropogenic Dust ' , Environmental Science & Technology , vol. 56 , no. 2 , þÿ p p . 7 6 1 7 6 9 . h t t p s : / / d o i . o r g / 1 0 . 1 0 2 1 / a c s . e s t . 1 c 0 4 7 7 9

http://hdl.handle.net/10138/341962
https://doi.org/10.1021/acs.est.1c04779

Environmental Science & Technology

pubs.acs.org/est

Article

Double Trouble of Air Pollution by Anthropogenic Dust

Wenwen Xia, Yong Wang,* Siyu Chen,* Jianping Huang, Bin Wang, Guang J. Zhang, Yue Zhang, Xiaohong Liu, Jianmin Ma, Peng Gong, Yiquan Jiang, Mingxuan Wu, Jinkai Xue, Linyi Wei, and Tinghan Zhang

Cite This: *Environ. Sci. Technol.* 2022, 56, 761−769

Read Online

ACCESS | Metrics & More | Article Recommendations | Supporting Information

ABSTRACT: With urbanization worldwide in recent decades, anthropogenic dust (AD) emissions due to heavy urban construction and off-road vehicle use have been increasing. Its perturbations on urban air pollution at the global scale are still unclear. Based on observations, we found that a high urban AD optical depth is often accompanied by severe non-dust aerosol optical depth in the planetary boundary layer (PBL), both magnitudes even comparable. To investigate the causes, an AD emission inventory constrained by satellite retrievals is implemented in a global climate model. The results show that AD-induced surface radiative cooling of up to −15.9 ± 4.0 W m^{-2} regionally leads to reduced PBL height, which deteriorates non-dust pollution, especially over India and northern China, in addition to the tremendous direct AD contribution to pollutants. The estimated global total premature mortality due to AD is 0.8 million deaths per year and is more severe in populous regions.

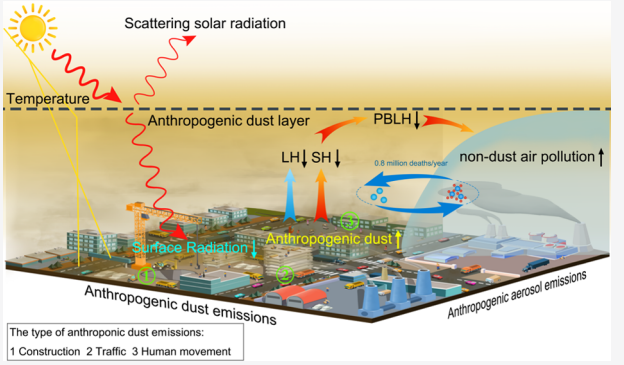

KEYWORDS: *anthropogenic dust, aerosol radiative forcing, planetary boundary layer, air pollution, premature mortality*

INTRODUCTION

Dust is a suspension of tiny mineral particles in the atmosphere, accounting for ∼70% of aerosol loading in the atmosphere. It can absorb and reflect solar and terrestrial radiation,[1,2] and alter cloud lifetime and cloud albedo by acting as efficient ice nuclei and cloud condensation nuclei.[3−7] Dust also contributes to air pollution. In addition to a direct contribution to $PM_{2.5}$ (particulate matter with diameters less than 2.5 μm) concentrations and a domination of PM_{10} (particulate matter with diameters less than 10 μm) concentrations,[8] dust can indirectly elevate non-dust anthropogenic pollutants by altering atmospheric circulation. In recent years, the most current studies commonly focused on the physical processes of natural dust (ND) over arid and semiarid regions and its environmental and climatic impacts. Numerical modeling and observations have found that natural East Asian dust emissions intensify non-dust air pollution in eastern China by weakening surface winds.[9] Surface cooling induced by radiative reflection and absorption of atmospheric dust can stabilize the planetary boundary layer (PBL), thus suppressing transboundary transport of air pollutants and leading to an explosive rise in near-surface $PM_{2.5}$ concentrations.[10,11]

In the early 1990s, Penner et al.[12] and Tegen and Fung[13] pointed out that it is inaccurate to merely classify dust aerosols as natural aerosols. Dust aerosols are supposed to be categorized into ND and anthropogenic dust (AD) according to different source regions and emission mechanisms.[14] ND is suspended in the atmosphere by strong winds and originates primarily from arid and semiarid regions with dry and unvegetated soils. AD is directly emitted from human activities in urban areas due to rapid urbanization with intense traffic, infrastructure construction, heavy building, and road construction.[15,16] The urban world is experiencing a sharp rise in $PM_{2.5}$, and AD has become increasingly abundant in the atmosphere in recent decades,[17] accounting for ∼30 to 70% of total dust concentrations in urban areas.[15,18] In this regard, the detection and quantification of AD were developed at the local and global scales.[15,19,20] However, previous studies significantly underestimated AD emissions and their impacts on urban air pollution, climate forcing, and human health.

Based on a linear relationship between AD emissions and dust sources of human interference and a simplified radiative transfer model, the global mean AD shortwave radiative effects of −0.46 W m^{-2} were estimated,[21] while Tegen et al.[22]

Received: July 20, 2021
Revised: November 26, 2021
Accepted: November 29, 2021
Published: December 23, 2021

estimated a global mean of 0.1 W m^{-2} at the top-of-atmosphere and up to −1.0 W m^{-2} at the surface, which is comparable to the magnitude of surface radiative cooling due to ND and other anthropogenic aerosols. AD has been seriously underestimated or ignored in global climate models (GCMs) to date,[23,24] which is probably attributed to the immature AD emission inventory. Therefore, the global cloud radiative effects (CRE) of AD have not been estimated, leading to the considerable uncertainties of the radiative budget in the Earth system. Additionally, given that anthropogenic pollutants are mainly emitted over urban areas, whether a linkage between urban AD and non-dust air pollutants exists remains unclear.

In densely populated urban regions, long-term exposure to high AD concentrations can create serious human health risks, including chronic obstructive pulmonary disease, lung cancer, acute lower respiratory infections, ischemic heart disease, and cerebrovascular disease.[25−28] Among the 1.1 million total $PM_{2.5}$-induced deaths in India in 2015, ∼99 900 deaths were attributed to AD. Additionally, in future projections, the increases in population-weighted dust concentrations and the associated human health impact are entirely attributed to AD changes.[29] However, there are abundant studies about the health effects related to ND rather than AD. Some studies focused on the health risks of road dust in high urban density areas (e.g., Guangzhou in China and Asturias in Spain) based on the risk assessment modeling of the United States Environmental Protection Agency or the Dutch National Institute of Public Health and Environmental Protection. They are considered as inducing both noncarcinogenic and carcinogenic risks. Combined with the exposure parameters of the local population,[30,31] the bioavailability of road dust in various particle sizes,[32] and the geochemical behavior effects of road dust,[33,34] the modeling assesses the carcinogenic and noncarcinogenic risks for children and adults exposed to road dust from ingestion, inhalation, and dermal contact pathways. However, to date, there are no studies quantitatively providing evaluations on the health risks related to AD at a global scale. The associated AD health effects, especially over medium urban density areas and remote regions due to weaker environmental regulations, poorer land management, and/or more intensive construction, are still unclear.

METHODS

Climate Model. The climate model used in this study is the National Center for Atmospheric Research (NCAR) Community Earth System Model version 1.2.1 (CESM1.2.1). The atmosphere model is the Community Atmosphere Model version 5.3 (CAM5.3), which has a finite-volume (FV) dynamical core[35] with a default horizontal resolution of 1.9° × 2.5° and a vertical resolution of 30 levels from the surface to 3.6 hPa. The three-mode version of the Modal Aerosol Module (MAM3)[36] is utilized to represent the properties and life cycle of major aerosol species (e.g., mineral dust, sea salt, sulfate, black carbon, primary organic matter, and secondary organic aerosol). The aerosol size distributions are represented by three log-normal modes: Aitken, accumulation, and coarse modes. MAM3 treats aerosols in Aitken mode with a diameter bound at 0.01−0.1 μm, accumulation mode at 0.1−1.0 μm, and coarse mode at 1.0−10.0 μm. Different aerosol species are internally mixed in each mode and externally mixed among different modes. CAM5 predicts the mass mixing ratios and the number mixing ratio of different aerosols for each mode.

The Dust Entrainment and Deposition Model (DEAD)[37] is embedded in CESM1.2.1 to parameterize mineral dust emissions. The dust emission scheme is based on a saltation and sandblasting process that is dependent on wind friction velocity, soil moisture, vegetation, and snow cover, all of which are strongly tied to the land model, Community Land Model version 4 (CLM4). CAM5 uses a soil erodibility factor described in Zender et al.,[38] which is globally heterogeneous, to take the susceptibility of various soil types to wind erosion into account. For MAM3, dust aerosols are emitted into the accumulation and coarse modes in the atmosphere with mass fractions of 0.032 and 0.968, respectively. The two-moment parameterization[39] (MG08) scheme is used to represent large-scale stratiform cloud microphysics.[40] Aerosols acting as CCN and IN in cirrus clouds are considered by Abdul-Razzak et al.[40] and Liu et al.,[41] respectively, in the MG08 scheme. Nonetheless, heterogeneous ice nucleation in mixed-phase clouds is not linked to aerosols and is dependent on air temperature only.[42] To consider dust and black carbon aerosols in heterogeneous ice nucleation in mixed-phase clouds, a classical nucleation theory-based heterogeneous ice nucleation scheme[5] is implemented (see below). Deep convection is parameterized using the Zhang−McFarlane (ZM) scheme,[43] and shallow convection parameterization uses the Park and Bretherton scheme.[44] The treatment of stratus−radiation−turbulence interactions is based on the Bretherton and Park scheme.[45] The radiative transfer is calculated using the Rapid Radiative Transfer Model (RRTM).[46]

Classical Nucleation Theory-Based Heterogeneous Ice Nucleation Scheme. The heterogeneous ice nucleation parameterization[5] is based on the classical nucleation theory (CNT), which parameterizes heterogeneous ice nucleation in mixed-phase clouds as a function of air temperature, nucleation time, contact angle, and the number concentrations of dust and soot aerosols. A single contact angle model is used to represent dust and soot aerosols participating in deposition nucleation, immersion, condensation, and contact freezing except for dust immersion freezing, which uses the probability density function (PDF) of the contact angle to represent diverse ice nucleation abilities among different dust particles. Uncertain parameters in the scheme are constrained by laboratory measurements. With this parameterization, the impact of AD as ice nucleating particles on mixed-phase clouds can be quantified.

AD Emission Inventory. An urban AD emission inventory based on a mutually developed environmental-stress model under constraints of CALIPSO is constructed.[15] To comprehensively reflect the intensity of human activities, the parameterization links population density, urbanization level, production and consumption of goods, and economic development level to AD emissions.[15,47,48] The STIRPAT (STochastic Impacts by Regression on Population, Affluence, and Technology) model was utilized to simulate AD emissions' inventory. The urbanization was estimated via the CNLI, and the economic development was quantified using GDP growth and Engel's coefficient (EC). EC is one of the classical parameters to measure the affluence of a region, which could well be associated with AD emissions.[47] The AD emissions in urban areas, G (μg m^{-2} s^{-1}), are given as follows

https://doi.org/10.1021/acs.est.1c04779
Environ. Sci. Technol. 2022, 56, 761−769

$$G = \begin{cases} 13.25 \times P^{0.12} \times \mathrm{GDP}_{\mathrm{growth}}^{0.006} \times \mathrm{EC}^{1.67}, & 0.0 < \mathrm{CNLI} \le 0.1 \\ 13.33 \times P^{0.05} \times \mathrm{GDP}_{\mathrm{growth}}^{0.01} \times \mathrm{EC}^{1.37}, & 0.1 < \mathrm{CNLI} \le 0.3 \\ 12.79 \times P^{0.08} \times \mathrm{GDP}_{\mathrm{growth}}^{0.01} \times \mathrm{EC}^{1.15}, & 0.3 < \mathrm{CNLI} \le 1.0 \end{cases} \quad (1)$$

where P is population density, $\mathrm{GDP}_{\mathrm{growth}}$ is the growth of gross domestic product reflecting the production and consumption per capita, EC is Engel's coefficient representing the proportion of total food expenditure to the total amount of consumer spending, which reveals the stage of economic development, and CNLI is a compounded night light index to quantify urbanization level.

Experimental Setup Based on the CALIPSO Constrained AD Emission. Like other anthropogenic aerosol emissions mainly emitted over urban areas from industrial, domestic, and agriculture activity sectors and implemented in GCMs as emission inventories,[49] an urban AD emission inventory constructed by Chen et al.[15] under constraints of CALIPSO retrievals is introduced into the NCAR Community Atmosphere Model version 5 (CAM5). The emitted AD mass fractions into the accumulation and coarse modes differ from the default MAM3 allocation (i.e., 0.032 and 0.968) because more fine particles are expected for AD compared with natural dust. Here, we assume that the mass fraction of AD emitted into the accumulation mode is more than that of natural dust by a relative increase of 20% (i.e., 0.032 × 1.2 = 0.038), based on an approximate estimate from previous studies.[50] The simulations (ADU) with the AD emission map are conducted to compare with control simulations (CTL), while both of them use Atmospheric Model Intercomparison Project (AMIP) type of configuration and are conducted at a 1.9°×2.5° horizontal resolution and a vertical resolution of 30 levels. In the ADU run, the dust optical properties for natural and anthropogenic dust are assumed to be the same except the particle size distribution, the uncertainty of which is examined by conducting the sensitivity simulations (see below). Both CTL and ADU simulations have 10 members differing only in the initial conditions by applying random round-off level errors (on the order of 10^{-14} °C) to the initial air temperature fields.[51] All simulations are forced annually by the prescribed, seasonally varying climatological present-day (averaged over 1982−2001) sea surface temperatures and sea ice extent data and are run for 6 years. Other anthropogenic aerosols and aerosol precursor emissions (e.g., sulfate and black carbon) are fixed at climatological present-day levels (averaged over 1982−2001) in both CTL and ADU simulations. Therefore, the increased AOD and reduced surface radiative fluxes are influenced by the introduction of anthropogenic dust emissions only. The first year in each simulation is discarded as the spin-up period. The ensemble means of dust concentrations and optical depth in ADU simulations minus those in the CTL simulation can approximate AD concentrations and optical depth, especially over AD source regions. Additionally, sensitivity tests are performed for the AD particle size distribution. One test follows the default MAM3 natural dust allocation (ADU−20), and the other test has a relative 20% increase in the mass fraction in the accumulation mode compared with the ADU run (ADU+20). As in CTL and ADU simulations, sensitivity tests have the same simulation setup and the same number of ensembles. All experiments are summarized in Table S1.

AD DRF and CRF. The AD DRF is estimated as $\Delta(F - F_{\mathrm{clean}})$, where Δ is the difference between ADU and CTL runs, which only differs if AD emissions are considered, F is net radiative flux (including both shortwave and longwave components) at the TOA or the surface, and F_{clean} is a diagnostic net radiative flux but neglects absorption and scattering of radiation by aerosols. The AD CRF is calculated as $\Delta(F_{\mathrm{clean}} - F_{\mathrm{clean,clear}})$, where $F_{\mathrm{clean,clear}}$ is an additional diagnostic net radiative flux that neglects the absorption and scattering of radiation by both aerosols and clouds.

Health-Impact Assessment. The $PM_{2.5}$-induced premature mortality (ΔM) was estimated using an epidemiological model. We calculated the health risks (i.e., chronic obstructive pulmonary disease, lung cancer, ischemic heart disease, and cerebrovascular disease) of long-term exposure to $PM_{2.5}$. The change in premature deaths is calculated by eq 2[52]

$$\Delta M = \frac{\mathrm{RR} - 1}{\mathrm{RR}} \times B \times P \quad (2)$$

where B is the cause-specific baseline mortality rate obtained from the GBD study of the baseline death incidence of a given health effect derived from the GBD database (http://www.healthdata.org/gbd/data) and P is the exposed gridded population obtained from the Gridded Population of the World dataset version 3 (GPWv3, http://sedac.ciesin.columbia.edu/gpw) supported by the Center for the International Earth Science Information Network and the Centro International de Agricultural Tropical. RR is the relative risk for cause-specific mortality. We used the method provided by GBD (the Global Burden of Disease Study) to calculate the RR on grid points from the AD_{25} concentrations obtained in this work. The relevant parameters were obtained from GBD 2010 and Chen et al.[48]

$$\mathrm{RR}(C) = \begin{cases} 1 + \alpha[1 - \exp(-\gamma(C - C_0)^{\delta}], & C > C_0 \\ 1, & C \le C_0 \end{cases} \quad (3)$$

where C is the annual mean simulated $PM_{2.5}$ concentration; C_0 is the theoretical minimum risk exposure level; and α, γ, and δ are parameters used to describe the shape of the concentration-response curve.[53]

CALIPSO ADOD. Natural dust from deserts and Gobi deserts could be deposited to remote regions through long-term transport. However, AD in urban areas is hard to lift to the PBL for long-range transport. The atmospheric AD loading is generally contributed by local AD emissions, and the technique for distinguishing AD from natural dust is based on CALIPSO dust, PBL height retrievals, and land-use and land-cover data sets.[18] The data of the extinction backscattering coefficient of the Level 1 product at 532 nm, the vertical profile of the depolarizing ratio and color ratio, and the data of the vertical feature mask (VFM) of the Level 2 product were used to detect AD optical depth (ADOD). In particular, a total of four steps were used to distinguish ADOD based on CALIPSO products in the study: obtaining the total dust optical depth (DOD) by CALIPSO; determining the global boundary layer height using CALIPSO retrievals; and determining the

https://doi.org/10.1021/acs.est.1c04779
Environ. Sci. Technol. 2022, 56, 761−769

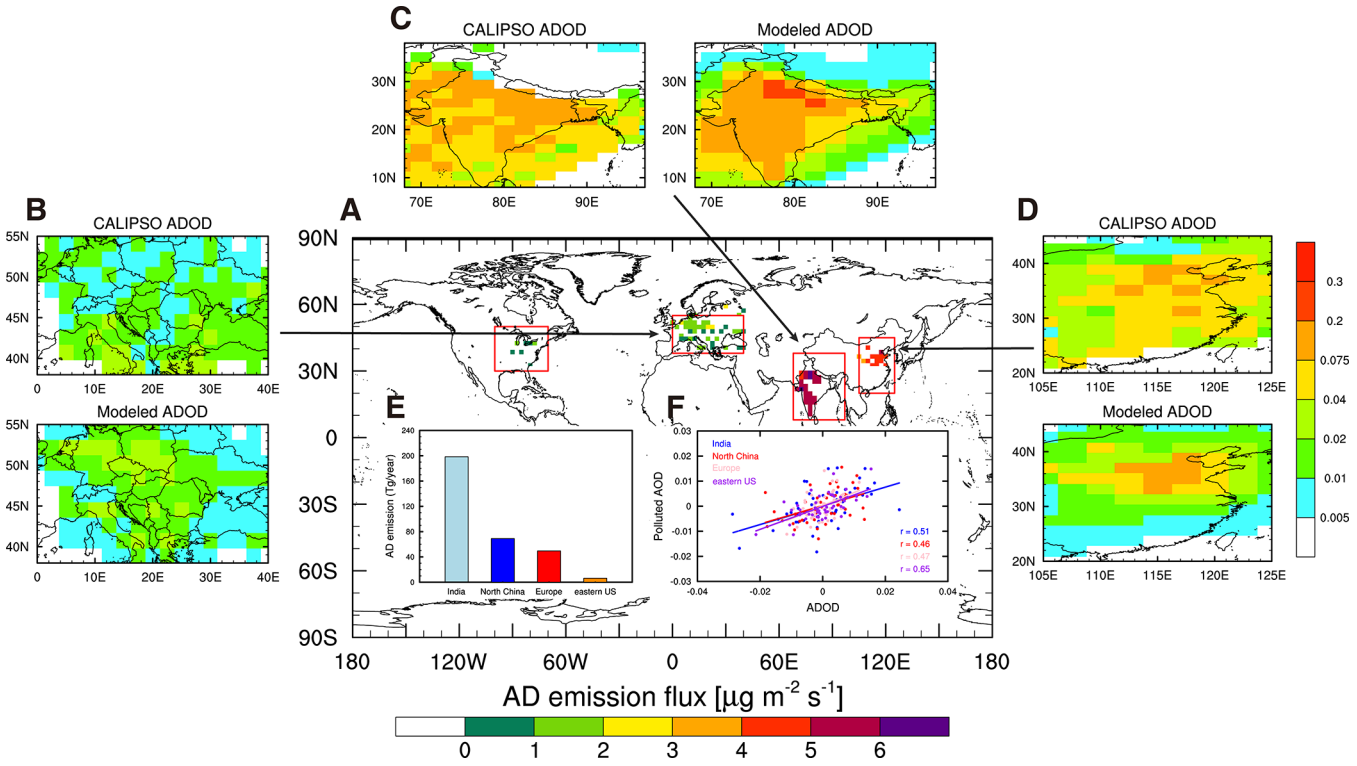

Figure 1. AD emissions and ADOD and its relationship with non-dust air pollution. (A) Global distribution of AD emission fluxes (μg m^{-2} s^{-1}). (B–D) CALIPSO-observed and simulated ADOD over Europe (B), India (C), and North China (D). (E) Total annual mean AD emissions (Tg year^{-1}) over India, North China, Europe, and the eastern US. (F) Observed relationship between ADOD and vertically integrated extinction coefficient of non-dust polluted aerosols below 500 m.

moderate resolution imaging spectroradiometer (MODIS) land cover to determine the AD source area at the global scale. Finally, according to dust optical properties, the natural dust generated by transmission and settlement within the boundary layer on the anthropogenic surface is removed to obtain the ADOD. Validated by field observations, the CALIPSO-derived ADOD well captures the global distributions of AD especially in urban areas of developing countries.[15,19,47] A detailed description of AD retrievals is provided in Huang et al.[18]

RESULTS

Urban AD and Associated Non-dust Air Pollutants. India, northern China, Europe, and the eastern United States are the four main urban AD source regions (Figure 1A). Correlation coefficients of 0.51, 0.46, 0.54, and 0.63 (all passing the 95% confidence level using the Student's t-test) between anthropogenic dust optical depth (ADOD) and the vertically integrated extinction coefficient of non-dust aerosols in the PBL over these regions are found in the Cloud-Aerosol Lidar and Infrared Pathfinder Satellite Observations (CALIPSO) (from January 2007 to December 2010), respectively (Figure 1F). Their optical depth anomalies are comparable. These findings imply that heavy urban AD not only substantially contributes to total air pollutants but also exacerbates severe non-dust air pollutants, implying double trouble of air pollution by AD. To determine the linkage, same as other anthropogenic aerosol emissions mainly emitted over urban areas from industrial, domestic, and agriculture activity sectors and implemented in GCMs as emission inventories,[49] an AD emission inventory constructed by Chen et al.[15] under constraints of CALIPSO retrievals is implemented in the NCAR CAM5 (see the Methods section). It is the first time that urban AD emissions are considered in a GCM. From the two simulations with and without the AD emissions (see the Methods section), the simulated ADOD is derived. India and China, two major developing countries, have the largest AD emission fluxes, showing 5.58 ± 0.03 and 4.55 ± 0.10 μg m^2 s^{-1}, respectively (Figure 1A). The AD emission fluxes in developed regions (i.e., western Europe and the eastern US) are considerably lower, at ~1.21 μg m^{-2} s^{-1}. For the annual total emission, India can reach as high as 200 Tg/year, while the eastern US just has around 5 Tg/year (Figure 1E). The simulated ADOD is comparable with CALIPSO retrievals over the four polluted regions (Figures 1B–D and S1).

We note that the vertical profile of the dust extinction coefficient in the simulation with AD emissions (referred to as ADU) agrees better with that in CALIPSO than the control model run (referred to as CTL) (Figure S2). In the CTL run, over the four regions, the dust extinction coefficient is underestimated at all of the altitudes, which is effectively increased in the ADU run closer to the observations, especially in India, China, and Europe. Additionally, at many aerosol robotic network (AERONET) sites over the four regions, the underestimation of aerosol optical depth (AOD) in the CTL run is alleviated in the ADU run (Figure S3). With a more realistic simulation of ADOD, AOD, and the vertical profile of dust extinction coefficient after the introduction of AD emissions in the model, the reasons for the relationship between AD and non-dust air pollutants in the PBL are further investigated below.

Attribution to AD Direct Radiative Forcing and Associated PBL Height Decrease. AD induces direct

https://doi.org/10.1021/acs.est.1c04779
Environ. Sci. Technol. 2022, 56, 761–769

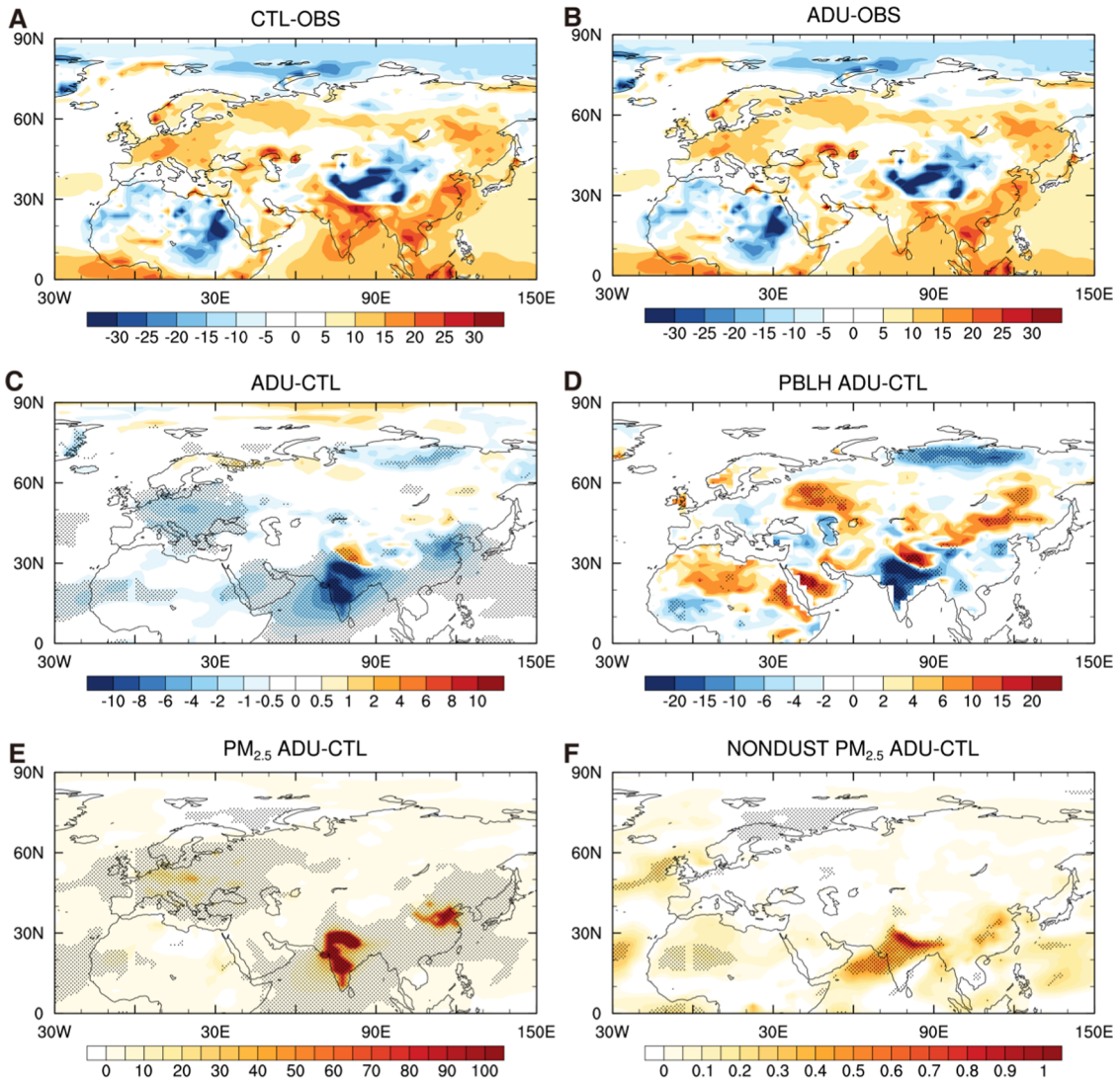

Figure 2. Clear-sky surface net shortwave flux, PBLH, and air pollutants. (A, B) Global distributions of biases in clear-sky surface net shortwave flux in CTL (A) and ADU (B) compared with CERES observations. (C−F) Global distributions of differences in clear-sky surface net shortwave flux (W m^{-2}) (C), PBL height (m) (D), $PM_{2.5}$ concentrations ($\mu g\ m^{-3}$) (E), and non-dust $PM_{2.5}$ concentrations (F) between ADU and CTL. Areas exceeding the 95% *t*-test confidence level in (C−F) are stippled.

radiative cooling at the surface over the four regions (Figure 2C), which is most significant over India by up to −15.9 ± 4.0 W m^{-2} (mean±one standard deviation) followed by over China and Europe (the United States is not shown because of the low AD emission and negligible enhancement of dust extinction coefficient). Accordingly, the positive biases of the simulated clear-sky surface net shortwave flux over India in the CTL run are effectively mitigated compared with the Clouds and the Earth's Radiant Energy System (CERES) observations (averaged over 2005−2015) (Figure 2A,B). At the top-of-atmosphere (TOA), similar regional improvements are found (Figure S4), although the global means between the two simulations are comparable (287.9 W m^{-2} in ADU versus 288.0 W m^{-2} in CTL). The global mean direct radiative forcing (DRF) due to AD at the surface in this study is −0.20 ± 0.15 W m^{-2} smaller than −1.0 W m^{-2} estimated by Tegen et al.[22] It is because the AD particles in Tegen et al.[22] include those dust particles from disturbed soils by human activities, some of which, to some extent, are still considered to be natural dust particles in GCMs. The global mean AD DRF at the surface over land is −0.40 ± 0.29 W m^{-2}, falling into the uncertainty range of −0.08 to −0.9 W m^{-2} provided by Sokolik and Toon.[21] The global mean DRF at the TOA in this study is −0.07 ± 0.12 W m^{-2}, agreeing well with −0.14 W m^{-2} in Stanelle et al.[54] and the documented value of −0.10 ± 0.20 W m^{-2} in the International Panel on Climate Change Assessment Report 5 (IPCC AR5).[55] As a response to the reduced clear-sky surface shortwave radiation, the sensible and latent heat fluxes are substantially reduced over India (Figure S5), thus profoundly decreasing the PBL height (Figure 2D). Besides India, northern China and Europe also experience decreases in the PBL height but with smaller magnitudes due to fewer AD emissions (Figure 1A,E).

Elevated Air Pollutants and Human Health Risks. The stabilized PBL over India traps more non-dust air pollutants in the PBL, suppressing their transboundary transport (Figure 2F). With the smaller decreases of the PBL height, northern China and Europe bear comparatively fewer non-dust air pollutants. More severely, along with the direct contribution of AD to total $PM_{2.5}$ concentrations, air quality deteriorates

https://doi.org/10.1021/acs.est.1c04779
Environ. Sci. Technol. 2022, 56, 761−769

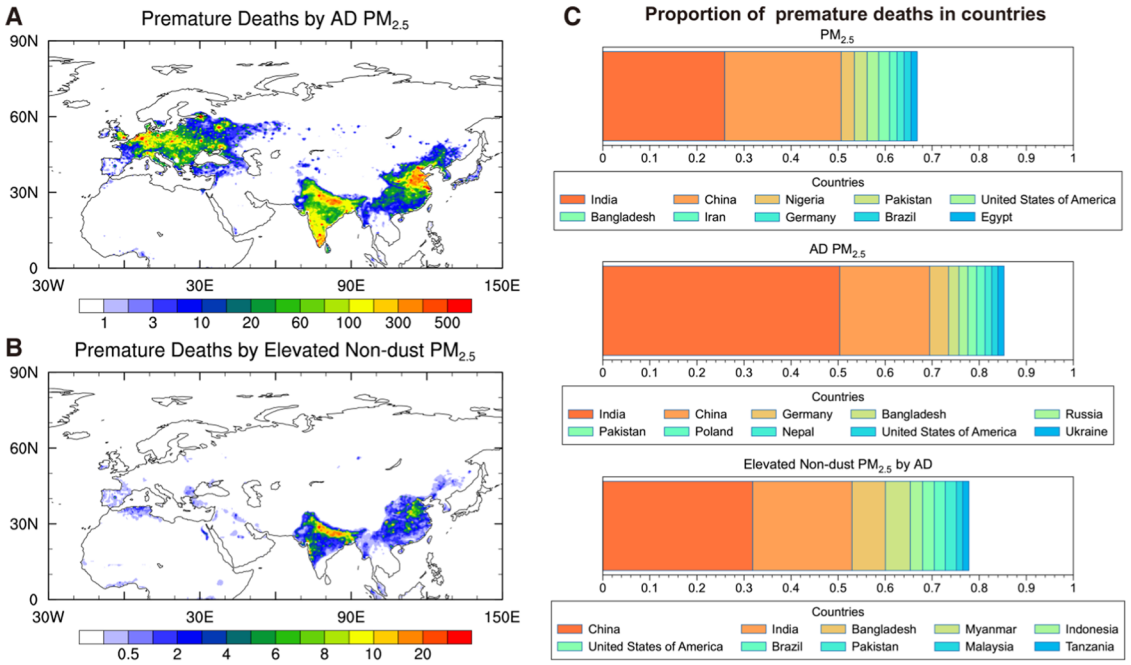

Figure 3. Premature deaths. (A, B) Global distributions of premature deaths (deaths per 1000 km^2 per year) caused by elevated AD (A) and non-dust $PM_{2.5}$ concentrations (B). (C) Proportion of premature deaths at the country level caused by elevated total $PM_{2.5}$, AD $PM_{2.5}$, and non-dust $PM_{2.5}$.

sharply in India, exceeding 100 μg m^{-3} (Figure 2E), and suggesting that the direct contribution of AD to the total air pollutants is much larger than its indirect contribution through aerosol−radiation−PBL interactions. Note that the inclusion of AD emissions over India makes the simulated total $PM_{2.5}$ concentrations agree better with the observations (Figure S6). Due to the dominant role of the direct contribution induced by AD, it is inevitable that northern China also experiences a dramatic increase in air pollutants, followed by Europe. As expected, air pollutants by AD over these regions are more serious in boreal winter (Figure S7).

With elevated air pollutants, AD deteriorates human health, causing 0.8 million premature deaths globally per year which is estimated by an integrated exposure-response (IER) model (see the Methods section). In particular, over the densely populated and highly urbanized regions of India and China, premature deaths that are directly due to AD exceed 4000 deaths/1000 km^2 (Figure 3A). The estimated global total premature mortality resulting from increased non-dust air pollutants in the PBL is ∼7000 deaths per year, although the regional values are low (Figure 3B). At the national level, China and India together bear more than 50% of premature deaths worldwide, resulting from elevated total $PM_{2.5}$ concentrations in which India directly suffers from approximately half of the health risks from AD pollutants worldwide (Figure 3C). Additionally, for non-dust air pollution in the PBL, premature deaths in India and China also account for more than 50% of the deaths worldwide.

DISCUSSION

The climatic and health effects of AD are investigated by observations and modeling. Besides AD sources from rapid urbanization with traffic intensities, infrastructure construction, heavy building, and road construction considered, AD can also be emitted from human-modified or disturbed land, such as wind erosion over croplands, pasturelands, grasslands, and dry lakes.[15] The reasons for excluding these sources in the model are described as follows. On the one hand, the contribution of urban AD to total AD is dominant over all four regions. On the other hand, there is still a debate on how to separate AD from natural dust sources in GCMs. Some studies still group dust emitted over croplands from wind erosion into natural dust sources.[14]

Another uncertainty of this study arises from the AD particle size distribution. Since AD has more fine particles in the atmosphere than natural dust,[15] we assume a relative increase by 20% for the mass fraction of fine particles of AD emitted into the atmosphere compared with that of natural dust based on an approximate estimate from the previous studies.[50] As different sizes of dust particles have distinct radiative properties, the impact of this uncertainty is investigated by conducting sensitivity simulations (see the Methods section). Overall, with sensitivity simulations, changes in the vertical profile of the dust extinction coefficient and clear-sky net shortwave flux at the surface caused by this perturbation in the size distribution can be neglected (Figures S2 and S8), implying that the uncertainty of the AD particle size distribution has negligible impacts on our conclusions.

Unlike AD direct DRF, large uncertainties exist in AD cloud radiative forcing (CRF) as well as associated liquid and ice water paths.[35] Nonetheless, they are still explored qualitatively. Overall, there are no significant changes in CRF at the TOA and the surface, and liquid and ice water paths (Figure S9C−F). Despite this, directly linked to AD, increases in cloud condensation nuclei number concentrations occur in source regions, such as India and northern China, while an increase in ice nuclei number concentrations is found over the Tibetan Plateau with low air temperature, and the Indian AD is transported there (Figure S9A,B).

AD directly contributes to $PM_{2.5}$ and can also indirectly elevate it through its additionally imposed surface radiative cooling, which traps more non-dust air pollutants as the PBL

https://doi.org/10.1021/acs.est.1c04779
Environ. Sci. Technol. 2022, 56, 761−769

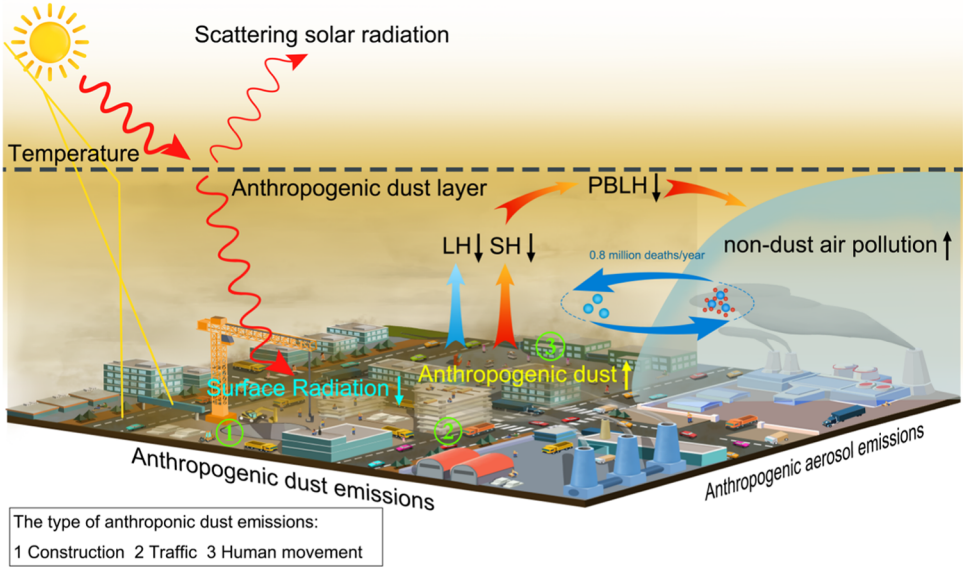

Figure 4. Schematic diagram. AD emissions over urban areas and subsequent climate and human health impacts. Anthropogenic dust emissions inventories include urban dust sources from intense traffic, infrastructure construction, heavy building, and road construction. Anthropogenic aerosol emissions refer to those sources for non-dust aerosols including sulfate, nitrate, black carbon, organic carbon, and others which come from fossil and nonfossil fuel burning, transportation, and various industrial emissions. Here, PBLH stands for planetary boundary layer height, LH latent heat flux, SH sensible heat flux, and T air temperature. Note that the background picture of the urban canopy just indicates that the focus of this study is urban AD rather than reflects urban-scale simulations conducted.

height decreases. The mechanisms and consequences are summarized in Figure 4. These findings imply that even with the reduction of emissions for cleaner air in the future, AD emissions if not well limited can substantially damage associated benefits.

■ ASSOCIATED CONTENT

Supporting Information

The Supporting Information is available free of charge at https://pubs.acs.org/doi/10.1021/acs.est.1c04779.

Summarization of global climate model experiments (Table S1); evaluation of model simulations against observations (Figures S1−S4, S6, and S8); impacts of AD on heat fluxes (Figure S5); modeled $PM_{2.5}$ in boreal winter (Figure S7); and the AD cloud effects (Figure S9) (PDF)

■ AUTHOR INFORMATION

Corresponding Authors

Yong Wang − *Department of Earth System Science, Ministry of Education Key Laboratory for Earth System Modeling, Institute for Global Change Studies, Tsinghua University, Beijing 100084, China*; Email: yongw@mail.tsinghua.edu.cn

Siyu Chen − *Key Laboratory for Semi-Arid Climate Change of the Ministry of Education, Lanzhou University, Lanzhou 730000, China*; Email: chensiyu@lzu.eud.cn

Authors

Wenwen Xia − *Department of Earth System Science, Ministry of Education Key Laboratory for Earth System Modeling, Institute for Global Change Studies, Tsinghua University, Beijing 100084, China*

Jianping Huang − *Key Laboratory for Semi-Arid Climate Change of the Ministry of Education, Lanzhou University, Lanzhou 730000, China*

Bin Wang − *Department of Earth System Science, Ministry of Education Key Laboratory for Earth System Modeling, Institute for Global Change Studies, Tsinghua University, Beijing 100084, China; State Key Laboratory of Numerical Modelling for Atmospheric Sciences and Geophysical Fluid Dynamics, Institute of Atmospheric Physics, Chinese Academy of Sciences, Beijing 100029, China*

Guang J. Zhang − *Scripps Institution of Oceanography, La Jolla, California 92037, United States*

Yue Zhang − *Key Laboratory for Semi-Arid Climate Change of the Ministry of Education, Lanzhou University, Lanzhou 730000, China*

Xiaohong Liu − *Department of Atmospheric Sciences, Texas A&M University, College Station, Texas 77843, United States*

Jianmin Ma − *Laboratory for Earth Surface Processes, College of Urban and Environmental Sciences, Peking University, Beijing 100871, China*

Peng Gong − *Department of Earth System Science, Ministry of Education Key Laboratory for Earth System Modeling, Institute for Global Change Studies and Tsinghua Urban Institute, Tsinghua University, Beijing 100084, China; Department of Geography and Department of Earth Sciences, University of Hong Kong, Hong Kong 999077, China*

Yiquan Jiang − *CMA-NJU Joint Laboratory for Climate Prediction Studies, Institute for Climate and Global Change Research, School of Atmospheric Sciences, Nanjing University, Nanjing 210023, China*

Mingxuan Wu − *Atmospheric Sciences and Global Change Division, Pacific Northwest National Laboratory, Richland, Washington 99354, United States*

Jinkai Xue − *Key Laboratory for Semi-Arid Climate Change of the Ministry of Education, Lanzhou University, Lanzhou 730000, China*

Linyi Wei − *Department of Earth System Science, Ministry of Education Key Laboratory for Earth System Modeling,*

https://doi.org/10.1021/acs.est.1c04779
Environ. Sci. Technol. 2022, 56, 761−769

Institute for Global Change Studies, Tsinghua University, Beijing 100084, China

Tinghan Zhang − *Atmosphere Biosphere Cryosphere Interactions Group, Institute for Atmospheric and Earth System Research (INAR), University of Helsinki, FI-00560 Helsinki, Finland*

Complete contact information is available at: https://pubs.acs.org/10.1021/acs.est.1c04779

Author Contributions

S.C., J.H., and Y.W. conceived the idea. Y.W. designed the experiments and W.X. conducted the model simulations. W.X. and Y.Z. performed the analysis. W.X., Y.W., and S.C. interpreted the results and wrote the paper. All authors participated in the revision and editing of the paper.

Notes

The authors declare no competing financial interest.

CERES radiation data can be accessed online at https://ceres.larc.nasa.gov/. CALIPSO data is available from https://www-calipso.larc.nasa.gov. AERONET data is available at https://aeronet.gsfc.nasa.gov/new_web/data.html and observed $PM_{2.5}$ concentrations are from https://aqicn.org/data-platform/covid19. The CAM5 simulation data is provided in an public data repository Zenodo (https://doi.org/10.5281/zenodo.5764304). The CESM1.2.1 source code can be downloaded from the CESM official website http://www2.cesm.ucar.edu.

■ ACKNOWLEDGMENTS

This work is supported by the National Natural Science Foundation of China Grants 42175106, 41975126, and 91837103 and the National Key Research and Development Program of China Grant 2017YFA0604000. G.J.Z. is supported by the US Department of Energy (DOE), Office of Science, Biological and Environmental Research Program (BER) under Award Numbers DE-SC19373 and DE-SC0016504. X.L. is supported by the DOE Energy Exascale Earth System Model (E3SM) project. M.W. is supported by the US DOE, Office of Science, Office of Biological and Environmental Research, Earth and Environmental System Modeling program as part of the Energy Exascale Earth System Model (E3SM) project. The Pacific Northwest National Laboratory (PNNL) is operated for DOE by the Battelle Memorial Institute under Contract DE-AC05-76RLO1830.

■ REFERENCES

(1) Li, Z.; Lau, W. K.-M.; Ramanathan, V.; Wu, G.; Ding, Y.; Manoj, M. G.; Liu, J.; Qian, Y.; Li, J.; Zhou, T.; Fan, J.; Rosenfeld, D.; Ming, Y.; Wang, Y.; Huang, J.; Wang, B.; Xu, X.; Lee, S. -S.; Cribb, M.; Zhang, F.; Yang, X.; Zhao, C.; Takemura, T.; Wang, K.; Xia, X.; Yin, Y.; Zhang, H.; Guo, J.; Zhai, P. M.; Sugimoto, N.; Babu, S. S.; Brasseur, G. P. Aerosol and Monsoon Climate Interactions over Asia. *Rev. Geophys.* **2016**, *54*, 866−929.

(2) Balkanski, Y.; Schulz, M.; Claquin, T.; Guibert, S. Reevaluation of Mineral Aerosol Radiative Forcings Suggests a Better Agreement with Satellite and AERONET Data. *Atmos. Chem. Phys.* **2007**, *7*, 81−95.

(3) DeMott, P. J.; Sassen, K.; Poellot, M. R.; Baumgardner, D.; Rogers, D. C.; Brooks, S. D.; Prenni, A. J.; Kreidenweis, S. M. African Dust Aerosols as Atmospheric Ice Nuclei. *Geophys. Res. Lett.* **2003**, *30*, No. 1732.

(4) Lau, W. K. M.; Kim, K.-M.; Zhao, C.; Leung, L. R.; Park, S.-H. Impact of Dust-Cloud-Radiation-Precipitation Dynamical Feedback on Subseasonal-to-Seasonal Variability of the Asian Summer Monsoon in Global Variable-Resolution Simulations With MPAS-CAM5. *Front. Earth Sci.* **2020**, *8*, No. 226.

(5) Wang, Y.; Liu, X.; Hoose, C.; Wang, B. Different Contact Angle Distributions for Heterogeneous Ice Nucleation in the Community Atmospheric Model Version 5. *Atmos. Chem. Phys.* **2014**, *14*, 10411−10430.

(6) Kumar, P.; Nenes, A.; Sokolik, I. N. Importance of Adsorption for CCN Activity and Hygroscopic Properties of Mineral Dust Aerosol. *Geophys. Res. Lett.* **2009**, *36*, No. L24804.

(7) Shi, Y.; Liu, X. Dust Radiative Effects on Climate by Glaciating Mixed-Phase Clouds. *Geophys. Res. Lett.* **2019**, *46*, 6128−6137.

(8) Querol, X.; Pey, J.; Pandolfi, M.; Alastuey, A.; Cusack, M.; Pérez, N.; Moreno, T.; Viana, M.; Mihalopoulos, N.; Kallos, G.; Kleanthous, S. African Dust Contributions to Mean Ambient PM10 Mass-Levels across the Mediterranean Basin. *Atmos. Environ.* **2009**, *43*, 4266−4277.

(9) Yang, Y.; Russell, L. M.; Lou, S.; Liao, H.; Guo, J.; Liu, Y.; Singh, B.; Ghan, S. J. Dust-Wind Interactions Can Intensify Aerosol Pollution over Eastern China. *Nat. Commun.* **2017**, *8*, No. 15333.

(10) Miller, R. L.; Perlwitz, J.; Tegen, I. Feedback upon Dust Emission by Dust Radiative Forcing through the Planetary Boundary Layer. *J. Geophys. Res.* **2004**, *109*, No. D24209.

(11) Zhong, J.; Zhang, X.; Dong, Y.; Wang, Y.; Liu, C.; Wang, J.; Zhang, Y.; Che, H. Feedback Effects of Boundary-Layer Meteorological Factors on Cumulative Explosive Growth of PM2.5 during Winter Heavy Pollution Episodes in Beijing from 2013 to 2016. *Atmos. Chem. Phys.* **2018**, *18*, 247−258.

(12) Penner, J. E.; Charlson, R. J.; Schwartz, S. E.; Hales, J. M.; Laulainen, N. S.; Travis, L.; Leifer, R.; Novakov, T.; Ogren, J.; Radke, L. F. Quantifying and Minimizing Uncertainty of Climate Forcing by Anthropogenic Aerosols. *Bull. Am. Meteorol. Soc.* **1994**, *75*, 375−400.

(13) Tegen, I.; Fung, I. Contribution to the Atmospheric Mineral Aerosol Load from Land Surface Modification. *J. Geophys. Res.* **1995**, *100*, 18707−18726.

(14) Tegen, I.; Werner, M.; Harrison, S. P.; Kohfeld, K. E. Relative Importance of Climate and Land Use in Determining Present and Future Global Soil Dust Emission. *Geophys. Res. Lett.* **2004**, *31*, No. L05105.

(15) Chen, S.; Jiang, N.; Huang, J.; Zang, Z.; Guan, X.; Ma, X.; Luo, Y.; Li, J.; Zhang, X.; Zhang, Y. Estimations of Indirect and Direct Anthropogenic Dust Emission at the Global Scale. *Atmos. Environ.* **2019**, *200*, 50−60.

(16) Philip, S.; Martin, R. V.; Snider, G.; Weagle, C. L.; Donkelaar, A.; van Brauer, M.; Henze, D. K.; Klimont, Z.; Venkataraman, C.; Guttikunda, S. K.; Zhang, Q. Anthropogenic Fugitive, Combustion and Industrial Dust Is a Significant, Underrepresented Fine Particulate Matter Source in Global Atmospheric Models. *Environ. Res. Lett.* **2017**, *12*, No. 044018.

(17) Moulin, C.; Chiapello, I. Impact of Human-induced Desertification on the Intensification of Sahel Dust Emission and Export over the Last Decades. *Geophys. Res. Lett.* **2006**, *33*, No. L18808.

(18) Huang, J. P.; Liu, J. J.; Chen, B.; Nasiri, S. L. Detection of Anthropogenic Dust Using CALIPSO Lidar Measurements. *Atmos. Chem. Phys.* **2015**, *15*, 11653−11665.

(19) Chen, S.; Jiang, N.; Huang, J.; Xu, X.; Zhang, H.; Zang, Z.; Huang, K.; Xu, X.; Wei, Y.; Guan, X.; Zhang, X.; Luo, Y.; Hu, Z.; Feng, T. Quantifying Contributions of Natural and Anthropogenic Dust Emission from Different Climatic Regions. *Atmos. Environ.* **2018**, *191*, 94−104.

(20) Xi, X.; Sokolik, I. N. Quantifying the Anthropogenic Dust Emission from Agricultural Land Use and Desiccation of the Aral Sea in Central Asia. *J. Geophys. Res.* **2016**, *121*, 12270−12281.

(21) Sokolik, I. N.; Toon, O. B. Direct Radiative Forcing by Anthropogenic Airborne Mineral Aerosols. *Nature* **1996**, *381*, 681−683.

(22) Tegen, I.; Lacis, A. A.; Fung, I. The Influence on Climate Forcing of Mineral Aerosols from Disturbed Soils. *Nature* **1996**, *380*, 419−422.

(23) Wu, C.; Lin, Z.; Liu, X. The Global Dust Cycle and Uncertainty in CMIP5 (Coupled Model Intercomparison Project Phase 5) Models. *Atmos. Chem. Phys.* **2020**, *20*, 10401−10425.
(24) Wu, M.; Liu, X.; Yang, K.; Luo, T.; Wang, Z.; Wu, C.; Zhang, K.; Yu, H.; Darmenov, A. Modeling Dust in East Asia by CESM and Sources of Biases. *J. Geophys. Res.* **2019**, *124*, 8043−8064.
(25) Zhao, C.; Liu, X.; Leung, L. R.; Hagos, S. Radiative Impact of Mineral Dust on Monsoon Precipitation Variability over West Africa. *Atmos. Chem. Phys.* **2011**, *11*, 1879−1893.
(26) Soltani, N.; Keshavarzi, B.; Moore, F.; Tavakol, T.; Lahijanzadeh, A. R.; Jaafarzadeh, N.; Kermani, M. Ecological and Human Health Hazards of Heavy Metals and Polycyclic Aromatic Hydrocarbons (PAHs) in Road Dust of Isfahan Metropolis, Iran. *Sci. Total Environ.* **2015**, *505*, 712−723.
(27) Shen, H.; Huang, Y.; Wang, R.; Zhu, D.; Li, W.; Shen, G.; Wang, B.; Zhang, Y.; Chen, Y.; Lu, Y.; Chen, H.; Li, T.; Sun, K.; Li, B.; Liu, W.; Liu, J.; Tao, S. Global Atmospheric Emissions of Polycyclic Aromatic Hydrocarbons from 1960 to 2008 and Future Predictions. *Environ. Sci. Technol.* **2013**, *47*, 6415−6424.
(28) Du, Y.; Gao, B.; Zhou, H.; Ju, X.; Hao, H.; Yin, S. Health Risk Assessment of Heavy Metals in Road Dusts in Urban Parks of Beijing, China. *Procedia Environ. Sci.* **2013**, *18*, 299−309.
(29) GBD MAPS Working Group. *Burden of Disease Attributable to Major Air Pollution Sources in India*, Special Report 21; Health Effects Institute: Boston, 2018.
(30) Khademi, H.; Gabarrón, M.; Abbaspour, A.; Martínez-Martínez, S.; Faz, A.; Acosta, J. A. Environmental Impact Assessment of Industrial Activities on Heavy Metals Distribution in Street Dust and Soil. *Chemosphere* **2019**, *217*, 695−705.
(31) Hou, S.; Zheng, N.; Tang, L.; Ji, X.; Li, Y.; Hua, X. Pollution Characteristics, Sources, and Health Risk Assessment of Human Exposure to Cu, Zn, Cd and Pb Pollution in Urban Street Dust across China between 2009 and 2018. *Environ. Int.* **2019**, *128*, 430−437.
(32) Zhang, J.; Hua, P.; Krebs, P. The Build-up Dynamic and Chemical Fractionation of Cu, Zn and Cd in Road-Deposited Sediment. *Sci. Total Environ.* **2015**, *532*, 723−732.
(33) Gunawardana, C.; Egodawatta, P.; Goonetilleke, A. Role of Particle Size and Composition in Metal Adsorption by Solids Deposited on Urban Road Surfaces. *Environ. Pollut.* **2014**, *184*, 44−53.
(34) Jayarathne, A.; Egodawatta, P.; Ayoko, G. A.; Goonetilleke, A. Assessment of Ecological and Human Health Risks of Metals in Urban Road Dust Based on Geochemical Fractionation and Potential Bioavailability. *Sci. Total Environ.* **2018**, *635*, 1609−1619.
(35) Lin, S.-J. A. "Vertically Lagrangian" Finite-Volume Dynamical Core for Global Models. *Mon. Weather Rev.* **2004**, *132*, 2293−2307.
(36) Liu, X.; Easter, R. C.; Ghan, S. J.; Zaveri, R.; Rasch, P.; Shi, X.; Lamarque, J.-F.; Gettelman, A.; Morrison, H.; Vitt, F.; Conley, A.; Park, S.; Neale, R.; Hannay, C.; Ekman, A. M. L.; Hess, P.; Mahowald, N.; Collins, W.; Iacono, M. J.; Bretherton, C. S.; Flanner, M. G.; Mitchell, D. Toward a Minimal Representation of Aerosols in Climate Models: Description and Evaluation in the Community Atmosphere Model CAM5. *Geosci. Model. Dev.* **2012**, *5*, 709−739.
(37) Zender, C. S.; Bian, H.; Newman, D. Mineral Dust Entrainment and Deposition (DEAD) Model: Description and 1990s Dust Climatology. *J. Geophys. Res.* **2003**, *108*, No. 4416.
(38) Zender, C. S.; Newman, D.; Torres, O. Spatial Heterogeneity in Aeolian Erodibility: Uniform, Topographic, Geomorphic, and Hydrologic Hypotheses. *J. Geophys. Res.* **2003**, *108*, No. 4543.
(39) Morrison, H.; Gettelman, A. A New Two-Moment Bulk Stratiform Cloud Microphysics Scheme in the Community Atmosphere Model, Version 3 (CAM3). Part I: Description and Numerical Tests. *J. Clim.* **2008**, *21*, 3642−3659.
(40) Abdul-Razzak, H.; Ghan, S. J. A Parameterization of Aerosol Activation: 2. Multiple Aerosol Types. *J. Geophys. Res.* **2000**, *105*, 6837−6844.
(41) Liu, X.; Penner, J. E.; Ghan, S. J.; Wang, M. Inclusion of Ice Microphysics in the NCAR Community Atmospheric Model Version 3 (CAM3). *J. Clim.* **2007**, *20*, 4526−4547.
(42) Meyers, M. P.; DeMott, P. J.; Cotton, W. R. New Primary Ice-Nucleation Parameterizations in an Explicit Cloud Model. *J. Appl. Meteorol.* **1992**, *31*, 708−721.
(43) Zhang, G. J.; McFarlane, N. A. Sensitivity of Climate Simulations to the Parameterization of Cumulus Convection in the Canadian Climate Centre General Circulation Model. *Atmos. Ocean* **1995**, *33*, 407−446.
(44) Park, S.; Bretherton, C. S. The University of Washington Shallow Convection and Moist Turbulence Schemes and Their Impact on Climate Simulations with the Community Atmosphere Model. *J. Clim.* **2009**, *22*, 3449−3469.
(45) Bretherton, C. S.; Park, S. A New Moist Turbulence Parameterization in the Community Atmosphere Model. *J. Clim.* **2009**, *22*, 3422−3448.
(46) Iacono, M. J.; Delamere, J. S.; Mlawer, E. J.; Shephard, M. W.; Clough, S. A.; Collins, W. D. Radiative Forcing by Long-lived Greenhouse Gases: Calculations with the AER Radiative Transfer Models. *J. Geophys. Res.* **2008**, *113*, No. D13103.
(47) Guan, X.; Huang, J.; Zhang, Y.; Xie, Y.; Liu, J. The Relationship between Anthropogenic Dust and Population over Global Semi-Arid Regions. *Atmos. Chem. Phys.* **2016**, *16*, 5159−5169.
(48) Chen, S.; Zhang, X.; Lin, J.; Huang, J.; Zhao, D.; Yuan, T.; Huang, K.; Luo, Y.; Jia, Z.; Zang, Z.; Qiu, Y.; Xie, L. Fugitive Road Dust PM 2.5 Emissions and Their Potential Health Impacts. *Environ. Sci. Technol.* **2019**, *53*, 8455−8465.
(49) Lamarque, J.-F.; Bond, T. C.; Eyring, V.; Granier, C.; Heil, A.; Klimont, Z.; Lee, D.; Liousse, C.; Mieville, A.; Owen, B.; Schultz, M. G.; Shindell, D.; Smith, S. J.; Stehfest, E.; Aardenne, J. V.; Cooper, O. R.; Kainuma, M.; Mahowald, N.; McConnell, J. R.; Naik, V.; Riahi, K.; Vuuren, D. P. van. Historical (1850−2000) Gridded Anthropogenic and Biomass Burning Emissions of Reactive Gases and Aerosols: Methodology and Application. *Atmos. Chem. Phys.* **2010**, *10*, 7017−7039.
(50) Chiou, S.-F.; Tsai, C.-J. Measurement of Emission Factor of Road Dust in a Wind Tunnel. *Powder Technol.* **2001**, *118*, 10−15.
(51) Kay, J. E.; Deser, C.; Phillips, A.; Mai, A.; Hannay, C.; Strand, G.; Arblaster, J. M.; Bates, S. C.; Danabasoglu, G.; Edwards, J.; Holland, M.; Kushner, P.; Lamarque, J.-F.; Lawrence, D.; Lindsay, K.; Middleton, A.; Munoz, E.; Neale, R.; Oleson, K.; Polvani, L.; Vertenstein, M. The Community Earth System Model (CESM) Large Ensemble Project: A Community Resource for Studying Climate Change in the Presence of Internal Climate Variability. *Bull. Am. Meteorol. Soc.* **2015**, *96*, 1333−1349.
(52) Anenberg, S. C.; Horowitz, L. W.; Tong, D. Q.; West, J. J. An Estimate of the Global Burden of Anthropogenic Ozone and Fine Particulate Matter on Premature Human Mortality Using Atmospheric Modeling. *Environ. Health Perspect.* **2010**, *118*, 1189−1195.
(53) Burnett, R. T.; PopeIII, C. A.; Ezzati, M.; Olives, C.; Lim, S. S.; Mehta, S.; Shin, H. H.; Singh, G.; Hubbell, B.; Brauer, M.; Anderson, H. R.; Smith, K. R.; Balmes, J. R.; Bruce, N. G.; Kan, H.; Laden, F.; Prüss-Ustün, A.; Turner, M. C.; Gapstur, S. M.; Diver, W. R.; Cohen, A. An Integrated Risk Function for Estimating the Global Burden of Disease Attributable to Ambient Fine Particulate Matter Exposure. *Environ. Health Perspect.* **2014**, *122*, 397−403.
(54) Stanelle, T.; Bey, I.; Raddatz, T.; Reick, C.; Tegen, I. Anthropogenically Induced Changes in Twentieth Century Mineral Dust Burden and the Associated Impact on Radiative Forcing. *J. Geophys. Res.* **2014**, *119*, 13526−13546.
(55) Boucher, O.; Randall, D.; Artaxo, P.; Bretherton, C.; Feingold, G.; Forster, P.; Kerminen, V.-M.; Kondo, Y.; Liao, H.; Lohmann, U.; Rasch, P.; Satheesh, S. K.; Sherwood, S.; Stevens, B.; Zhang, X.-Y. Clouds and Aerosols. In *Climate Change 2013: The Physical Science Basis. Contribution of Working Group I to the Fifth Assessment Report of the Intergovernmental Panel on Climate Change*; Stocker, T. F.; Qin, D.; Plattner, G.-K.; Tignor, M.; Allen, S. K.; Boschung, J.; Nauels, A.; Xia, Y.; Bex, V.; Midgley, P. M., Eds.; Cambridge University Press: Cambridge, United Kingdom, 2013.

https://doi.org/10.1021/acs.est.1c04779
Environ. Sci. Technol. 2022, 56, 761−769